PAPER IN FOREFRONT

Smartphone-coupled three-layered paper-based microfluidic chips demonstrating stereoscopic capillary-driven fluid transport towards colorimetric detection of pesticides

Hongjiao Wu[1] · Jiaqi Chen[1] · Yi Yang[1] · Weitai Yu[1] · Ying Chen[1] · Pengcheng Lin[1] · Ke Liang[2]

Abstract

The existence of pesticide residues in the hydrosphere, biosphere, and anthroposphere can cause acute or chronic diseases and deteriorate the environment. Therefore, efficient detection of pesticide residues is of great significance to prevent food poisoning, control food pollution, and protect human lives by recognizing their distribution and concentration. Herein, a novel smartphone-coupled three-layered paper-based microfluidic chip is proposed as a facile platform to detect the pesticides. The stereoscopic capillary-driven fluid transport is enabled by the three-layered microfluidic chip configuration. The detection mechanism is based on the enzyme inhibition reaction and the chromatic reaction. The detection results are obtained by a smartphone and figured out by colorimetric quantitative analysis. Taking advantages of the above merits, we demonstrate the utilization of this smartphone-coupled three-layered paper-based microfluidic chip for the effective analysis of typical pesticides (profenofo and methomyl). The linear ranges of profenofo and methomyl are 0.27–2.1 µmol L^{-1} and 0.14–1.85 µmol L^{-1}, respectively. The corresponding limits of detection in the chips are 55 nM and 34 nM, respectively. The paper-based chips are also highly cost-effective with a total cost of 0.082 ¥ per piece. It can be anticipated that this technique will open new avenues for the mass fabrication of paper-based microfluidic chips and provide state-of-the-art methods in the field of analytical chemistry.

Keywords Microfluidic · Paper-based chip · Pesticide detection · Colorimetric · Quantitative analysis

Introduction

Pesticides are widely used in the development of agricultural production, especially in some developing countries [1, 2]. Pesticides can protect crops from pests in the process of growth and development, thus stabilizing and increasing the yield of crops. However, excessive pesticide and its degradation products will permeate into the soil, harden the soil, and cause environmental pollution in hydrosphere, biosphere, and anthroposphere [3]. Furthermore, pesticides can also accumulate in food, leading to food pollution and human health harm. Therefore, it is particularly important to develop a rapid and accurate method for the detection of pesticide residues [4, 5]. The conventional detection methods include the high-performance liquid chromatography, liquid chromatography-mass spectrometry [6], gas chromatography-mass spectrometry [7, 8], ion-exchange chromatography [9, 10], and fluorescence spectroscopy [11, 12]. Although these methods are highly sensitive, the preprocessing is complex, time-consuming, expensive, and labor-consuming, which requires professional personnel to operate and is difficult to meet the needs for real-time and rapid detection. Therefore, it is of great theoretical and practical significance to develop low-cost, convenient, efficient, and rapid detection methods towards the pesticide residues.

Microfluidic analysis is a new subject in the field of chemical analysis, medical diagnosis, safety detection, sample treatment, and micro-reaction [13–21]. It is a comprehensive science integrating chip manufacturing, microfluidic

✉ Pengcheng Lin
  pclin@gdut.edu.cn

✉ Ke Liang
  568849792@qq.com

[1] Guangdong Provincial Key Laboratory On Functional Soft Condensed Matter, School of Materials and Energy, Guangdong University of Technology, Guangdong 510006, China

[2] R&D Center, Guangdong Dayuan Oasis Food Safety Technology Co., LTD, Guangzhou 510530, China

mechanics, material transport physics, chemical reaction dynamics, spectroscopy, and modern informatics [22–24]. It can reduce the basic functions of chemical analysis and detection laboratory to a few square centimeter chip and strengthen the diffusion and collision between reactants. The microfluidic analysis is now presenting strong development vitality in aspects of accelerating the detection reaction speed, realizing the rapid, miniaturized, and automated procedure by integrating the sample processing and sample detection [25–27]. Among the various microfluidic chips, paper-based microfluidic chips have further promoted the miniaturization and integration of analytical laboratory since it was proposed, with the advantages of low cost, no external driving force, high portability, and environmental friendliness. Nowadays, they are widely used in the field of fixed-point medical treatment, environmental monitoring, and food on-site detection due to the visualization of detection results [28–32].

Previously, researchers have proposed the pesticide detection using the paper-based microfluidic chips. The silver nanoparticle decorated paper-based microfluidic chips are used to test the thiram and ferbam with subnanomolar sensitivity [33]. A nanoporous cellulose paper-based SERS platform with Gold nanorods is developed to analyze multiplex hazardous pesticides including thiram, tricyclazole, and carbaryl by surface-enhanced Raman scattering [34]. Nanoceria-coated paper-based devices as a detection platform are applied for the analysis of organophosphate pesticides in an enzyme inhibition assay with acetylcholinesterase and choline oxidase [35]. A paper-based three-electrode electrochemical biosensor with a mitochondria-modified Toray carbon paper working electrode can potentially be used as a portable platform for pesticides detection [36]. A rapid, on-site, and quantitative paper-based immunoassay platform with competitive indirect enzyme-linked immunosorbent assay is established for the efficient pesticide determination [37]. Food safety monitoring of the pesticide phenthoate can be achieved using a smartphone-assisted paper-based sensor with bimetallic Cu@Ag core–shell nanoparticles [38]. Although the paper-based detection platforms have been proved to be highly efficient in the quantitative analysis of the pesticides, specific nanoparticles and professional signal generation methods are essential in the detection procedures. The disadvantages of the above methods include the weak interaction between the surface-loaded nanoparticles and the hydrophilic paper, the additional functionalization of the paper chip, and the expensive signal acquisition instrument (SERS or ELISA). Therefore, it is of great significance to develop a low-cost, portable, and accurate detection method towards the pesticides.

Herein, a novel smartphone-coupled three-layered paper-based microfluidic chip is proposed as a facile colorimetric sensing platform to detect the pesticides. The three-layered paper-based microfluidic chips can be massively manufactured by wax printing and heat treatment (Fig. 1a). The stereoscopic capillary-driven fluid transport both in the horizontal plane and in the vertical direction is enabled by the three-layered microfluidic chip configuration, while the fluid transport is mainly confined in the horizontal plane for a single-layered chip. Another advantage of three-layered chip over the single-layered chip is the capacity to hold more liquid reagents and to avoid the liquid spilling out of the chip (Fig. 1b). The setup of the smartphone-coupled three-layered paper-based microfluidic device is listed in Fig. 1c. The detection mechanism is based on the enzyme inhibition reaction and the chromatic reaction (Fig. 1d). The three-layered paper-based microfluidic chip presents colorimetric qualitative analysis by naked eyes. Furthermore, the colorimetric images can be easily captured by a smartphone. Two types of image processing results (average gray value and average RGB value) are figured out for the data quantitative analysis. The proposed detection method is also highly cost-effective owing to the cheap chip materials and economical reagent dosage. Taking advantages of the above merits, we demonstrate the use of these smartphone-coupled three-layered paper-based microfluidic chip for the effective analysis of typical pesticides (profenofos and methomyl), showing superior linear detection ranges and low detection limits. This work provides a low-cost, portable, visual and sensitive analysis strategy for the efficient detection of pesticides. We hope that this technique will open new avenues for the large-scale fabrication of paper-based microfluidic chips and boost the state-of-the-art analysis methods in the future.

Experimental

Materials

Acetylcholine, 5,5′-Dithio bis-(2-nitrobenzoic acid) (DTNB), dipotassium hydrogen phosphate (K_2HPO_4), and potassium dihydrogen phosphate (KH_2PO_4) were purchased from Aladdin. Acetylcholine esterase was purchased from Guangdong Dayuan Oasis Food Safety Technology Co., Ltd. The standard solutions of profenofos (100 μg mL^{-1}, Acetone) and methomyl (100 μg mL^{-1}, Methanol) were provided by the Environmental Protection Research Institute of the Ministry of Agriculture. Whatman filter qualitative filter papers (Whatman No. 1) were obtained from Sigma Aldrich. Whatman No. 1 filter paper is a commercial paper with medium retention capacity and flow rate. Whatman No. 1 filter paper possesses an aperture of 11 μm and a density of 88 gm^{-2}. The water used in the experiment is deionized water. All reagents were directly used without further purification.
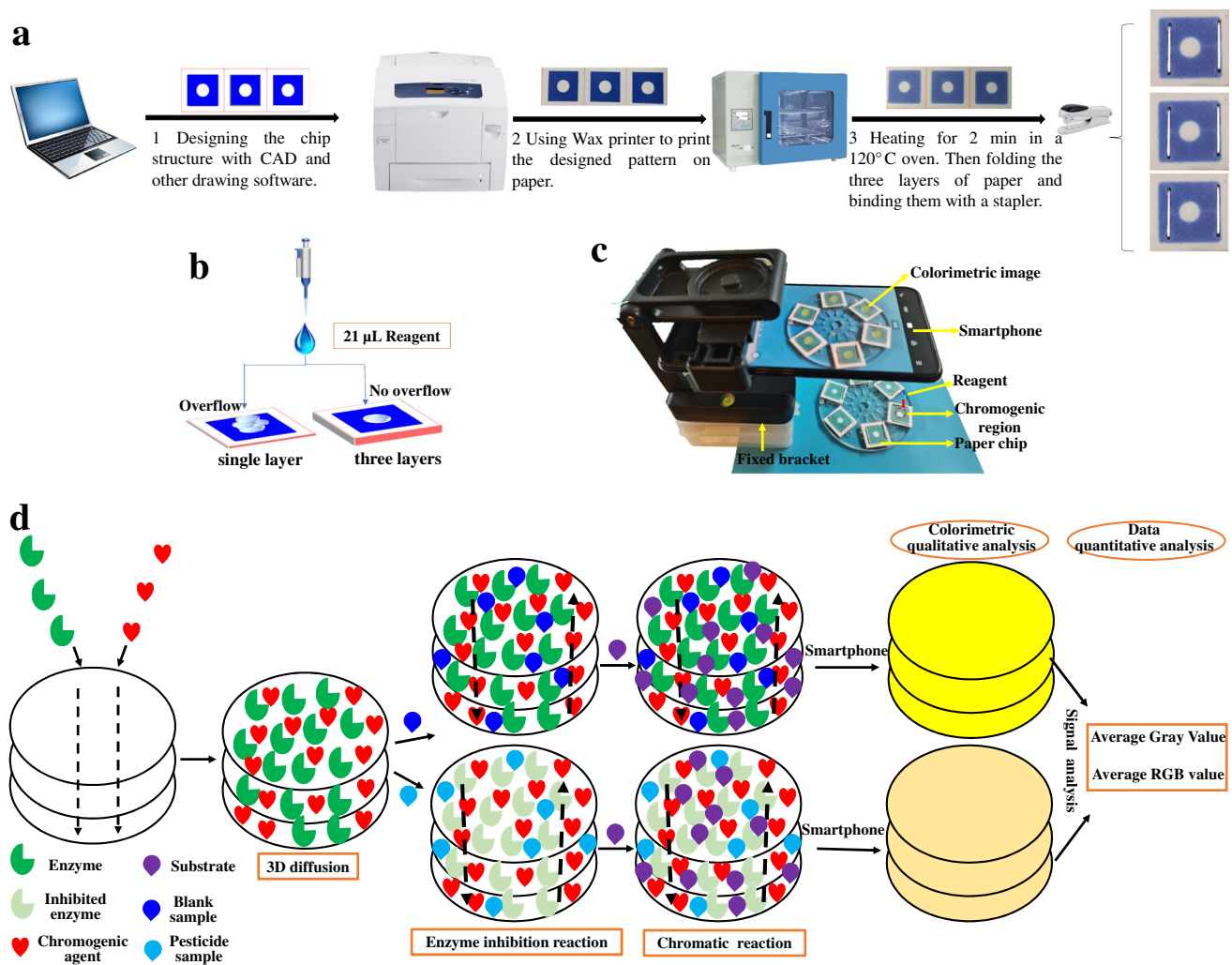
Fig. 1 Schematic illustration of the pesticide detection based on the smartphone-coupled three-layered paper-based microfluidic chip. **a** The fabrication process of three-layered paper-based microfluidic chip by wax printing and heat treatment. **b** The advantages of three-layered chip in avoiding the overflow of liquid reagents compared with single-layered chip. **c** The setup of the smartphone-coupled three-layered paper-based microfluidic device. **d** The three-dimensional transport of reagents, the enzyme inhibition reaction, chromatic reaction, the colorimetric qualitative analysis, and the data quantitative analysis of pesticide

Sample obtention and preparation

11.9 g of K_2HPO_4 and 3.2 g of KH_2PO_4 were mixed with 1000 mL of distilled water to prepare a NaH_2PO_4-Na_2HPO_4 buffer solution (0.1 M, pH 8.0). A stock solution for each pesticide (profenofos and methomyl) was first prepared in the buffer solution. The concentration of the stock solution is 1 µg mL^{-1}, and then the buffer solution was used to dilute the stock solution into a series of concentration. The concentrations of profenofos were 0.27 µmol L^{-1}, 0.54 µmol L^{-1}, 1.074 µmol L^{-1}, 1.61 µmol L^{-1}, and 2.1 µmol L^{-1}. The concentrations of methomyl are 0.14 µmol L^{-1}, 0.31 µmol L^{-1}, 0.62 µmol L^{-1}, 0.93 µmol L^{-1}, 1.24 µmol L^{-1}, and 1.85 µmol L^{-1}.

Fabrication of the paper-based chip

A wax printer (Xerox) was used to print the desired shape and manufacture hydrophobic barriers on the bulk paper. The architecture of the barriers was designed with the assistance of CorelDraw software. The paper chip was made up of three layers of unit paper chips with the same structure (dimensions are shown in Fig. 1). Each unit paper chip was a square with a side length of 10 mm composed of a hydrophilic detection area with a central diameter of 6 mm and a hydrophobic barrier area on the periphery. The printed paper was heated at 120 °C for 2 min. This allowed the wax to melt and penetrate the pores in the paper. The prepared paper chips with hydrophilic and hydrophobic areas were superimposed and bound with a stapler, so that each layer

was tightly combined to obtain a three-layered paper-based microfluidic chip.

Characterization of the paper-based chip

The morphologies and microstructures of paper-based chip were observed through SEM (S-3400 N, Hitachi). Fourier transform infrared (FTIR) spectra of the paper-based chip were captured by FTIR Spectrometer (iS50R, Nicolet) on a transmission mode. The contact angle measurement was performed using an optical angle meter system (OCA 15EC, Data Physics Instruments GmbH). The thermal stability of the samples was determined using a TGA (TG 209F1 Libra, NETZSCH) with a heating rate of 10 °C min^{-1} in a nitrogen atmosphere. The sample photos were taken by a digital camera (EOS700D, Canon).

Detection process of the pesticide on the paper-based chip

3 μL of enzyme, 3 μL of chromogenic reagent, and 12 μL of the tested sample were added to the detection area of the paper chip. After reacting for 5 min, 3 μL of substrate was added to the detection area. The color pictures of the detection reaction were taken by a smartphone and followed by imported into Photoshop and ImageJ to extract the average RGB value and average gray value of the color area. Acetylcholinesterase, acetylcholine (substrate), and DTNB (chromogenic agent) used in this paper are prepared according to the methods in the national standard of the People's Republic of China GB/T 5009.199–2003. The final concentrations of DTNB and acetylcholine are 2.9 M and 8.2 M, respectively. The final concentrations of the tested samples are described in Sample obtention and preparation. The main novelty of this work is to propose a smartphone-coupled three-layered paper-based microfluidic chip and verify the feasibility in the colorimetric detection of the pesticides. The selectiveness of the selected method can not be determined at this moment, which will be addressed in our future work when a variety of pesticides are ready.

Smartphone setup and data processing of the colorimetric images

For image acquisition, a smartphone (HUAWEI Nova7, HUAWEI Electronics, China) with a 64 million pixels camera (Photo quality 9000*6000 pixels) was employed. Throughout the optimization experiments, the photos were recorded using Open Camera v1.45.2 smartphone application (by Mark Harman). During the experimental operation, the smartphone was fitted on a holder facing the substrate from the top at a distance of 300 mm. Images were recorded under constant lighting conditions using an in-house fabricated enclosure. Imaging was done as soon as the sample was introduced on the substrate

for spot assays. The obtained photos were transferred to the PC and analyzed using ImageJ software (National Institutes of Health, USA). A circular region of interest (ROI) was selected and applied to each of the taken photos. Then the RGB measure function was used to obtain mean intensity of red, green, and blue channel in the selected ROI. To obtain histograms, a Color Histogram plug-in was used. The image color signal measurement index of ImageJ was changed to the average gray value. In this way, the corresponding measured value can be obtained. Finally, the average RGB value and average gray value were imported into the Origin (a function drawing software), and the data is fitted to obtain the linear relationship between each measurement value and the pesticide residue concentrations.

Calculation of the limit of detection (LOD)

The theoretical LOD is calculated according to the following formula,

$$LOD = \frac{3\sigma}{k} \tag{1}$$

where σ is the standard deviation of the average gray value and k is the slope of the linear equation.

Results and discussion

Characterization and analysis of paper-based chip

A three-layered paper-based microfluidic chip is fabricated by three consecutive steps of wax printing, thermal maturation, and folding assembly. The selected paper is commercial waterman NO1 cellulose paper. The length, width, and height of the obtained three-layered paper-based microfluidic chip are 10 mm, 10 mm, and 1 mm, respectively. The advantages of the proposed paper-based microfluidic chip over the previous plastic chips made of PDMS or PMMA include the low cost, easy processing, three-dimensional water transport, and capillary force driving without external pumps. The cellulose paper before wax printing demonstrates banded morphology with a length of hundreds of microns and a width of about 15 microns. The magnified SEM images show that the paper surface possesses fold and porous structure. The wax printing and thermal maturation obviously change the paper surface structure. The strip becomes thicker as the result of the wax infiltration and thermal expansion, with a width of about 20 microns. The magnified SEM image of the wax-loaded cellulose paper presents a flat and compact structure, which can effectively inhibit the wettability water. EDS mapping (Fig. 2d–f and Fig. 2j–l) indicates that the cellulose paper before and after the wax printing contains

Fig. 2 Morphology of the cellulosic paper before and after the wax printing. **a–f** SEM image, the magnified SEM image, and EDS mapping images of C, O, and P elements of cellulosic paper before the wax printing. **g–l** SEM image, the magnified SEM image and EDS mapping images of C, O, and P elements of cellulosic paper after the wax printing
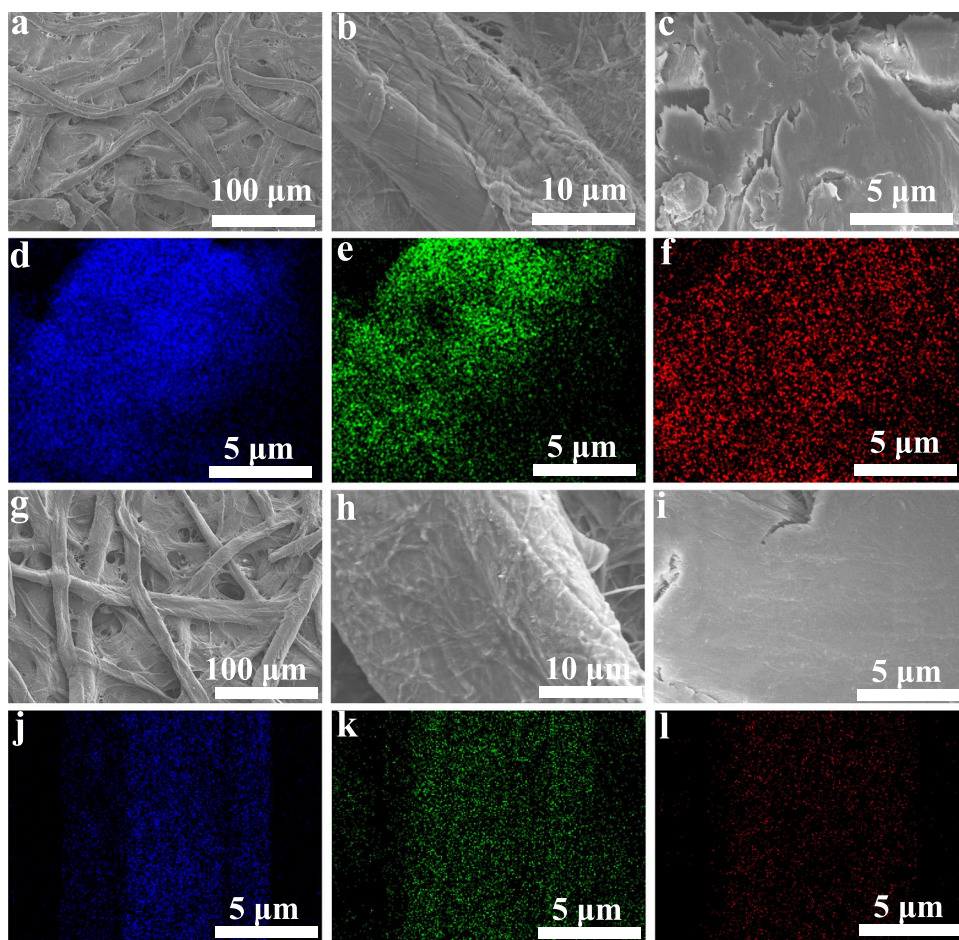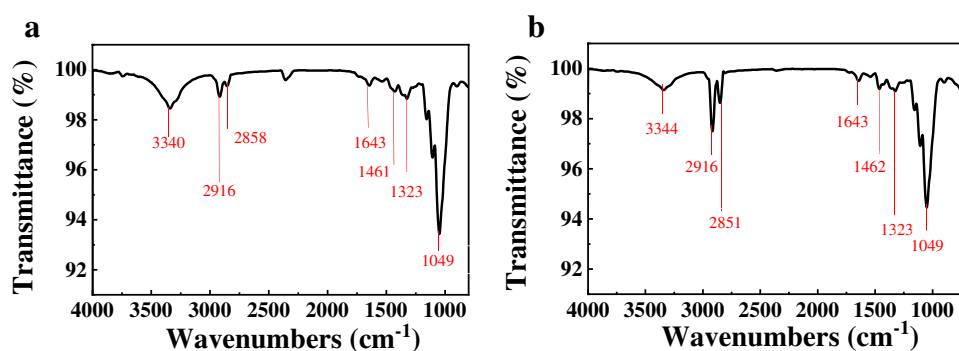

Fig. 3 a,b FT-IR spectra of the cellulosic paper before and after the wax printing

C, O, and P elements. It is worth noting that additional impurities are not introduced into the printed paper by wax printing and heat treatment, which is conducive to accurate detection.

The IR absorption spectra of neat cellulose paper and wax-loaded cellulose paper are listed in Fig. 3. The absorptions at 1049 cm^{-1} in the neat cellulose paper and wax-loaded cellulose paper are attributed to the stretching vibration of C-O. The absorptions at 2916 cm^{-1} and 2858 cm^{-1} in the neat cellulose paper are attributed to the stretching vibration of -CH$_2$. The absorptions at 2916 cm^{-1} and 2851 cm^{-1}

in the wax-loaded cellulose paper are also attributed to the stretching vibration of -CH$_2$. The absorptions at 3340 cm^{-1} in the neat cellulose paper and 3343 cm^{-1} in the wax-loaded cellulose paper are attributed to the stretching vibration of -OH. It is worth noting that the IR absorption of the cellulose paper after wax loading is almost the same as that of neat cellulose paper. This result can be ascribed to the following three reasons. One is that the chemical composition of the cellulose paper is not affected by the heat treatment in the chip manufacturing. The other is that no additional elements are introduced into the cellulose paper when loading
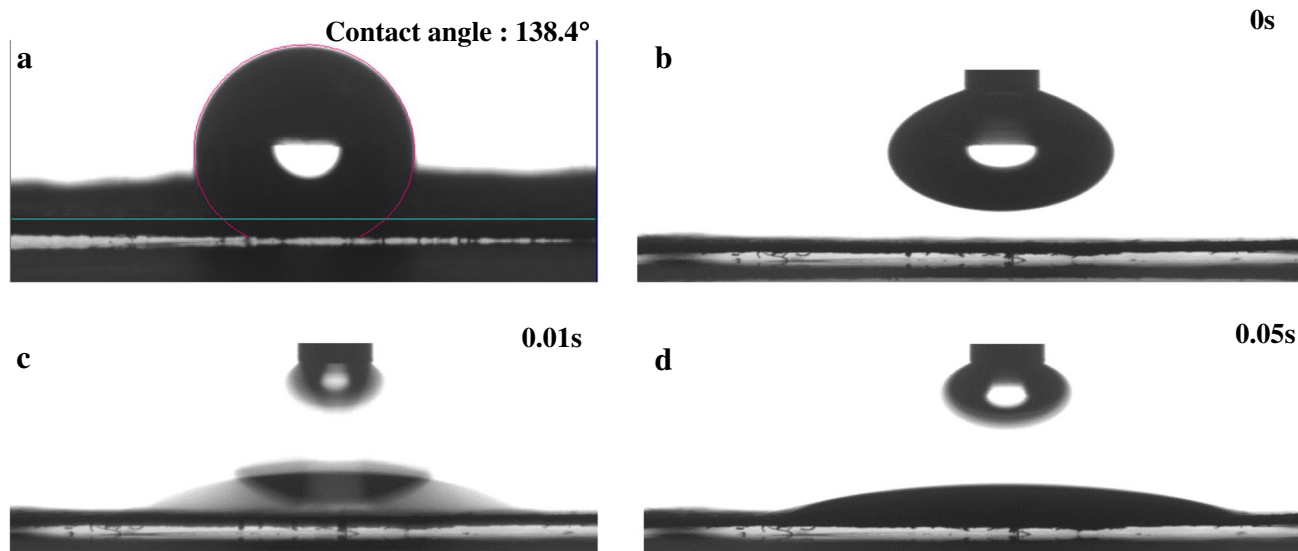
Fig. 4 The water wettability of the cellulosic paper before and after the wax printing. **a** The water contact angle of the cellulosic paper after the wax printing. **b–d** Time-dependent water contact angle of a water droplet on the flat cellulosic paper before the wax printing

the wax. The last one is that the combination between the cellulose paper and the wax is not chemical bonding. The wax is effectively infiltrated into the pores of the cellulose paper.

The water contact data are recorded to analyze the wetting property of the cellulose papers used for fabricating the three-layered paper-based microfluidic chip. The water contact angle of the wax-loaded cellulose paper is 138.4° as shown in Fig. 4a, demonstrating its poor affinity with water, whereas the original cellulose paper is highly hydrophilic. As shown in Fig. 4b–d, under ambient condition, a water droplet can be completely spread on the top of the original cellulose paper within 0.05 s as the result of the existence of abundant -OH groups and considerable internal holes to absorb the water. In order to quantify the instinct aqueous solution transport capacity of the neat.

cellulose paper and the wax-loaded cellulose paper, an aqueous solution transport experiment is carried out by observing the flow of the dye aqueous solution on the original cellulose paper. As shown in Fig. 5a, a drop of dye aqueous solution (50 μL) continuously flows on the neat cellulose paper with a spread speed of about 2.22 mm s^{-1}, proving the superior water transport capacity in the horizontal direction of the original cellulose paper. It is also noted that the color of the fluid fades gradually along the flow direction, indicating the superior water transport capacity in the vertical direction. In general, the capillary pumping and osmotic swelling effect enable the efficient three-dimensional water transport across the three-layered paper-based microfluidic chip. The dye aqueous solution is almost immobile on a flat wax-loaded cellulose paper when placed in a static state within 2 min (Fig. 5b). The size of the dye aqueous drop

remains basically unchanged. This result reveals that the aqueous solution can not be transported in the wax zone in the static condition. Furthermore, a drop of dye aqueous solution smoothly rolls on an inclined surface of the wax-loaded cellulose paper. The dye aqueous drop is not spread in the rolling process, indicating that the aqueous solution can not be transported in the wax zone in the dynamic condition (Fig. 5c). The significantly different water transport capacity of the original cellulose paper and the wax-loaded cellulose paper as above mentioned is conducive to the confined flow of the aqueous solution in the specific area of the paper-based microfluidic chip.

The effect of wax printing and thermal maturation on the thermal stability of cellulose paper is studied by investigating the degradation behavior of the original cellulose paper and the wax-loaded cellulose paper under a nitrogen atmosphere. The TGA curves and corresponding mass loss rates are plotted in Fig. 6; neat cellulose paper possesses excellent thermal stability when the temperature is below 200 °C due to the stable internal bonding of cellulose. The temperatures at 5 wt% weight loss of neat cellulose paper and wax-loaded cellulose paper are 289.8 °C and 323.0 °C, respectively. Meanwhile, the corresponding mass loss rates are listed in the inset of Fig. 6a; the temperatures at maximum mass loss rate (T_{max}) are respectively 354.3 °C and 360.8 °C. The increased degradation temperatures and T_{max} suggest that the thermal stability of paper is significantly enhanced after the incorporation of wax. The Horowits-Metzger integral kinetic equation is selected to examine the activation energy (E_a) for thermal decomposition [39].

Fig. 5 The water transport capacity of the cellulosic paper before and after the wax printing. **a** The transport of aqueous dye solution on the cellulosic paper before the wax printing. **b** The contact between aqueous dye solution and the cellulosic paper after the wax printing. **c** The sliding of a drop of aqueous dye solution on the cellulosic paper after the wax printing
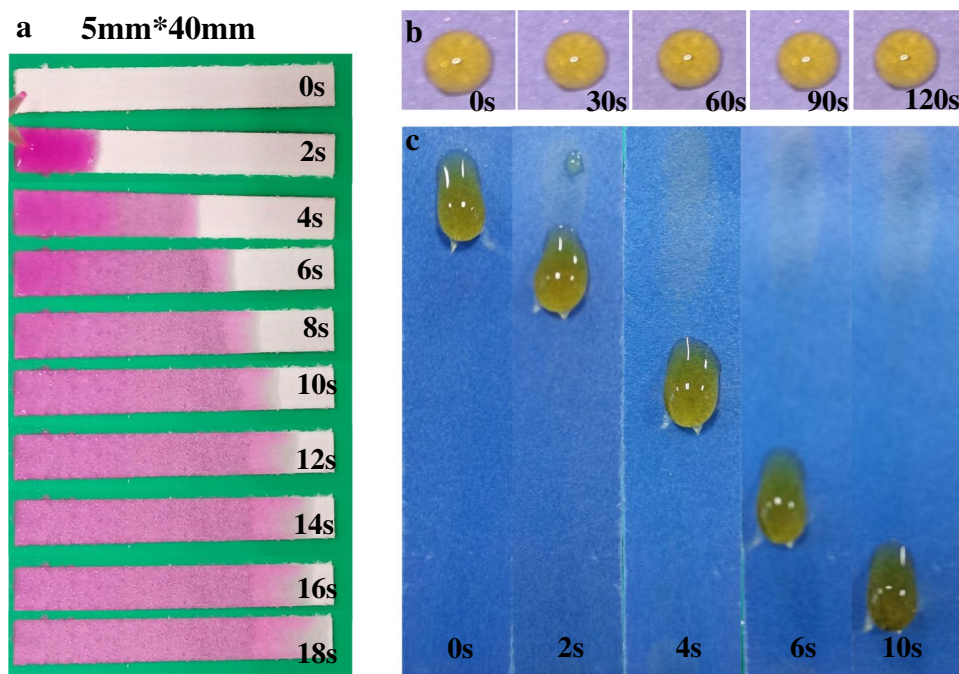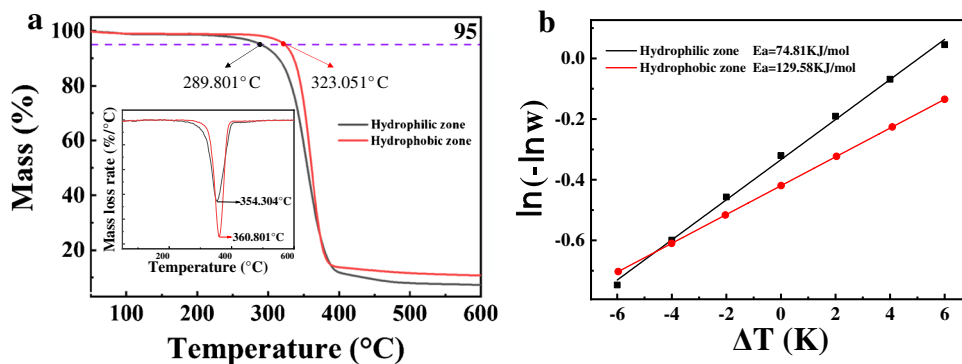
Fig. 6 Thermal stability analysis of the cellulosic paper before and after the wax printing. **a** TGA thermographs of the cellulosic paper before and after the wax printing. The inset shows the first derivatives of the TGA curves. **b** The plots of ln(−ln w) versus ΔT for the cellulosic paper before and after the wax printing

$$\ln(-lnm) = \frac{E_a \Delta T}{RT_{max}^2} + k \tag{2}$$

where m is the residual mass percentage, ΔT is defined as $\Delta T = T - T_{max}$, R is the universal gas constant 8.314 J mol^{-1} K^{-1}, and k is the intercept of the linear equation. The E_a values can be estimated from the slope of the plot of ln(-ln m) versus ΔT (see Fig. 6b). The E_a values of neat cellulose paper and wax-loaded cellulose paper are calculated to be 74.81 and 129.58 kJ mol^{-1}. The increased E_a can be attributed to the stable thermal stability of the wax and the interaction between the wax and cellulose paper. Meanwhile, the increased E_a values are also consistent with the increased decomposition temperatures, further proving that the incorporation of wax can enhance the thermal stability of cellulose paper.

Detection mechanism and process in the paper-based chip

The traditional quantitative detection of pesticide residues is conducted by expensive large instruments (ultraviolet–visible spectrophotometer, gas chromatography-mass spectrometry, liquid chromatography-mass spectrometry, and supercritical fluid chromatography). The development of quantitative detection based on paper-based chip is a highly affordable way to realize the portable detection in various public places, not just in the lab. The analysis of economic cost is calculated as follows. A piece of paper-based chip is mainly composed of detection reagents and paper-based materials. The reagent cost and the paper-based cost are 0.2 ¥/100 pieces and 8 ¥/100 pieces, respectively. Therefore, the total cost = reagent cost + paper-based cost = 8.2 ¥/100 pieces, demonstrating a highly cost-effective feature. After demonstration of the
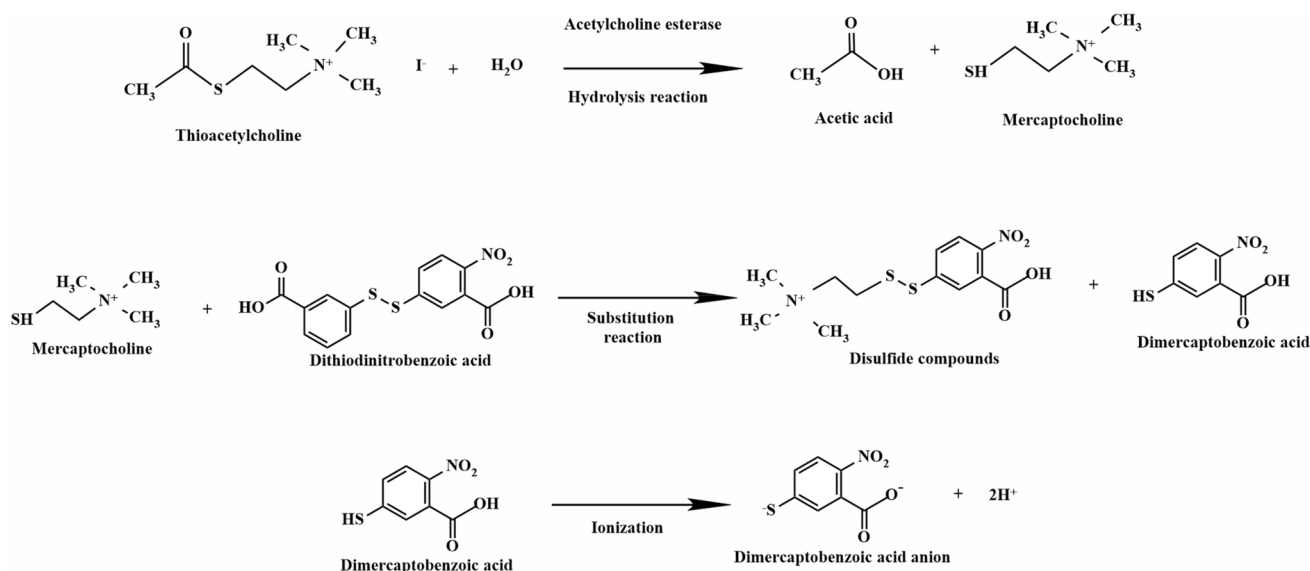
Fig. 7 The mechanism and process of pesticide residue detection in the paper-based chip including hydrolysis reaction, substitution reaction, and the ionization reaction

stereoscopic capillary-driven fluid transport on the hydrophilic paper and the completely inhibited water infiltration on the hydrophobic paper, we integrate the paper-based microfluidic chip with enzyme (acetylcholine esterase), chromogenic agent (DTNB), and substrate (acetylcholine) to form a facile platform for pesticide detection. The detection mechanism is based on the classical enzyme inhibition method (see Fig. 7). For a blank sample without the pesticides, the whole detection process consists of the following three steps. The substrate (acetylcholine) hydrolysis reaction is catalyzed by the acetylcholinesterase to produce the mercaptocholine, the substitution reaction between the chromogenic agent (DTNB) and mercaptocholine to generate the thiosalicylic acid, and the ionization reaction of thiosalicylic acid to form the corresponding yellow anions. For a positive sample containing the pesticides, the whole detection process consists of the four steps. The added step is the enzyme inhibition reaction before the above-mentioned three reactions. It is worth noting that the reaction activity of acetylcholinesterase is inevitably decreased after interacting with pesticides, presenting a reduced production of mercaptocholine, thiosalicylic acid, and the yellow ionic compounds. The detection procedure is started by adding 3 μL of acetylcholine esterase, 3 μL of DTNB, and 12 μL of sample solution in turn to the hydrophilic area in the three-layered paper-based chip. Then, the sample solution, acetylcholine esterase, and chromogenic agent are incubated within the hydrophilic area for 3 min to start the enzyme inhibition reaction. Finally, 3 μL of substrate solution (acetylcholine) is added on the hydrophilic area to start the hydrolysis reaction, substitution reaction, and ionization reaction. Since the reactions in the detection procedure

cause the color transition from colorless to yellow, the average gray values and the average values of red, green, and blue channel are utilized as the decisive parameters to evaluate the pesticide level. The accuracy of the average gray values and the average RGB values of the color pictures obtained by a smartphone is confirmed by image processing software (image J and Photoshop).

Establishment of standard curve for two typical pesticide residues (profenofos and methomyl)

Among various pesticides, profenofos (O-(4-bromo-2-chlorophenyl phosphorothioate) O-ethyl S-propyl) and methomyl (S-methyl-N-(methylcarbamoyloxy) thioacetimidate) possess developmental and reproductive toxicity [40–43]. Therefore, profenofos and methomyl are selected as representative pesticides for the detection in the paper-based chip. Firstly, the profenofos is taken as a pesticide sample to verify the validity of the paper chip detection. The color reaction is designed to be 15 min so as to finish the detection reaction. As shown in Fig. 8a, the three-layered paper chip presents a brilliant yellow after completing the color reaction when the concentration of the profenofos is 0 mg mL^{-1}. The displayed color is getting lighter and lighter when increasing the profenofos concentration in the samples. Two optical signal processing methods are proposed to extract the colorimetric signals from the color paper chip, namely, the average gray value obtained by image J and the average RGB value by photoshop. The calculated optical data demonstrate that the average gray value and the average RGB value are gradually increased when increasing the profenofos concentration from 0.27 to 2.1 μmol L^{-1},
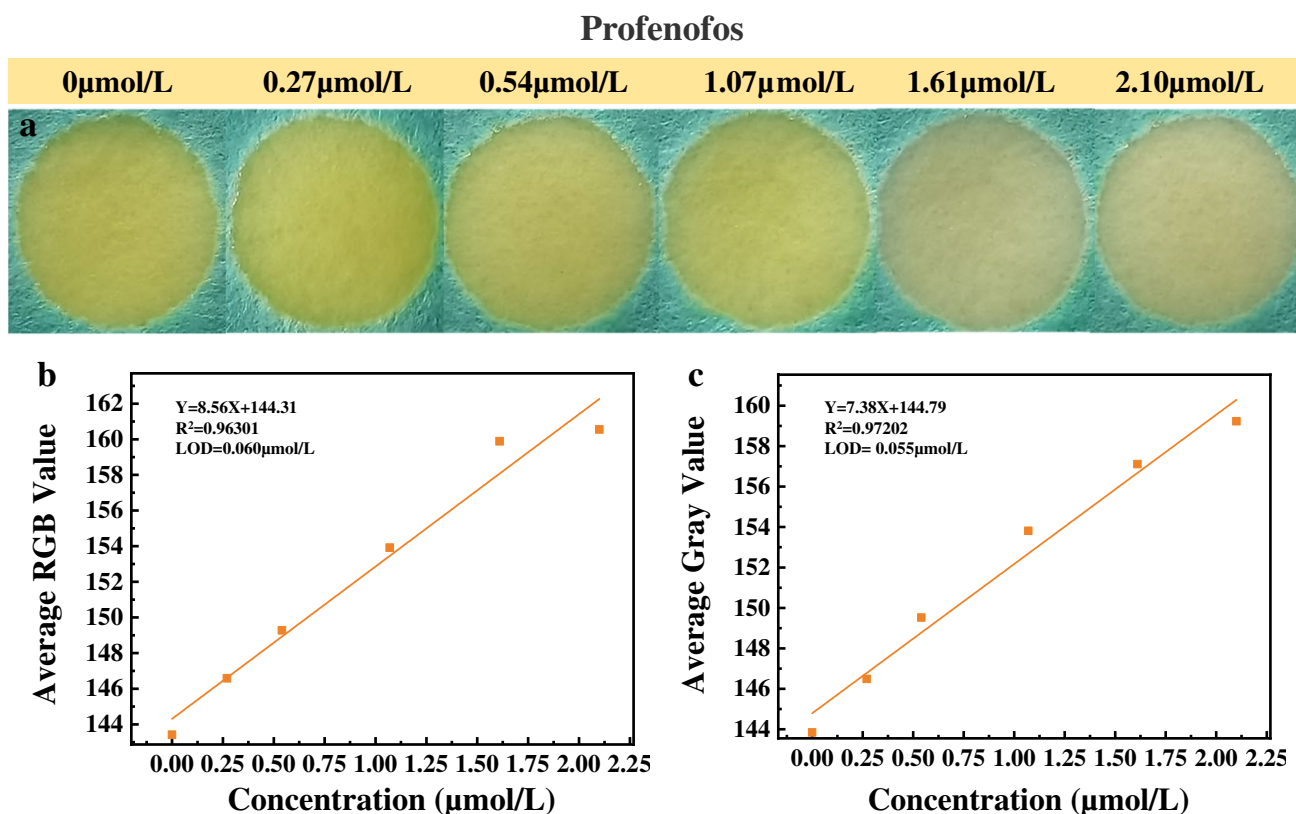
Profenofos

Fig. 8 Pesticide residue (profenofos) detection on the paper chip. **a** Optical images of the displayed color after the pesticide residue triggers the color reaction on the paper chip. **b** The linear relationship between the average RGB value and profenofos concentration. **c** The linear relationship between the average gray value and profenofos concentration

proving the excellent accuracy of detection. Therefore, we can establish a linear equation between the profenofos concentration and the average RGB value (the average gray value) of the paper chip as shown in Fig. 8b, c. The linear equations are determined to be $Y = 8.56X + 144.31$ and $Y = 7.38X + 144.79$ by using the average RGB value and the average gray value, respectively. The limits of detection can be calculated to be 60 nM and 55 nM based on 3σ/slope rule. Then, another pesticide sample methomyl is also selected to verify the validity of the paper chip detection. The color reaction is designed to be 10 min so as to finish the detection reaction. As shown in Fig. 9a, the three-layered paper chip presents a brilliant yellow after completing the color reaction when the concentration of the methomyl is 0.14 μmol L^{-1}. The displayed color is getting lighter and lighter when increasing the methomyl concentration in the samples. The calculated optical data demonstrate that the average gray value and the average RGB value are gradually increased when increasing the methomyl concentration from 0.14 to 1.85 μmol L^{-1}, proving the excellent accuracy of detection. Therefore, we can establish a linear equation between the methomyl concentration and the average RGB value (the average gray value) of the paper chip as shown in Fig. 9b, c. The linear equations are determined to

be $Y = 10.53X + 141.97$ and $Y = 10.22X + 141.67$ by using the average RGB value and the average gray value, respectively. The limits of detection can be calculated to be 36 nM and 34 nM based on 3σ/slope rule. It is worth noting that both profenofos and methomyl have also been detected by previous methods such as fluorescence polarization, surface-enhanced Raman scattering, gas chromatography, HPLC, LC–MS/MS, and electrochemistry. The corresponding LOD is listed in Table 1. It is worth noting that the color signal extraction will have errors when different types of mobile phones are used for image capturing. Therefore, the same mobile phone (HUAWEI Nova7, HUAWEI Electronics, China) with a 64 million pixels camera (Photo quality 9000*6000 pixels) is used in this work. An improved signal detector will be equipped to directly convert the color signal into the digital signal in our future work, which not only reduces the errors caused by the mobile phone, but also improves the convenience of the detector and is more suitable for on-site detection.

Detection of pesticide residues in real samples

After establishing the linear equation between the pesticide concentration and the optical signals, the pesticide detection
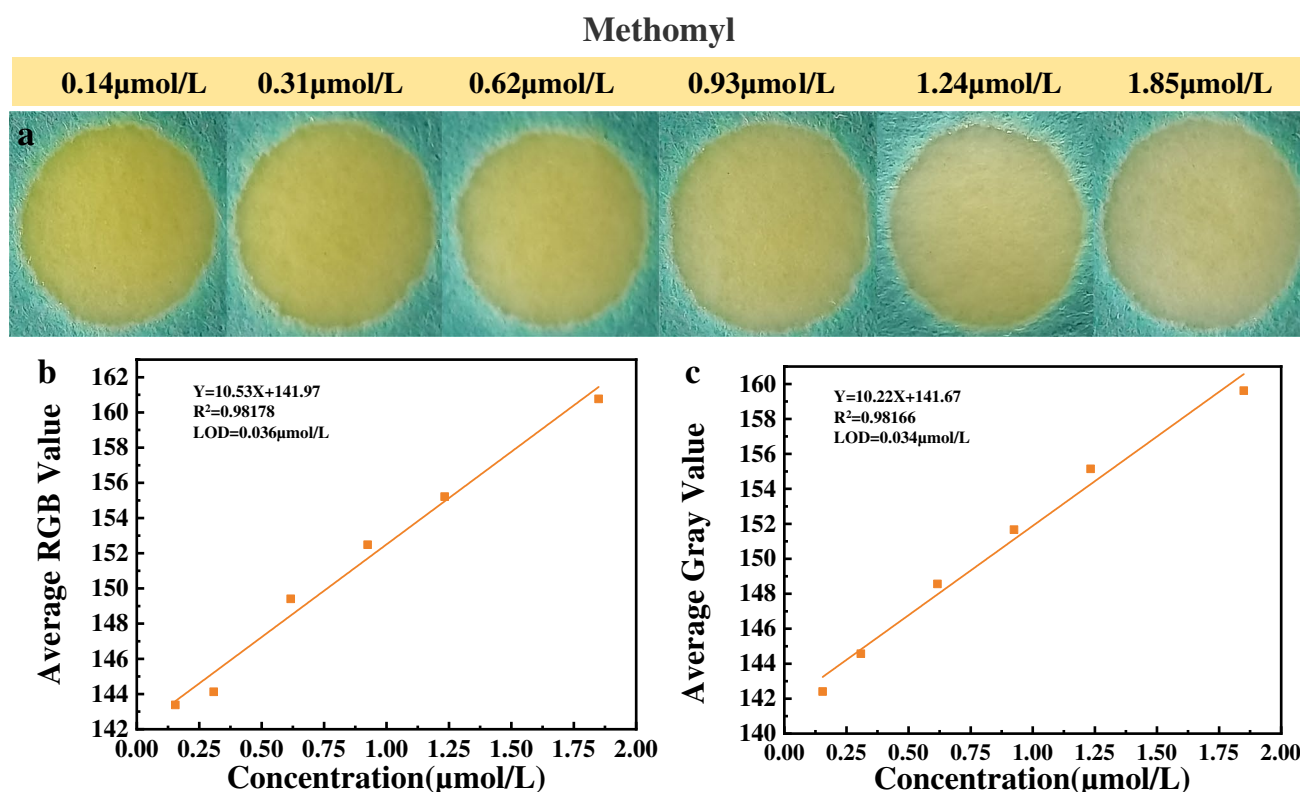
Methomyl

| 0.14µmol/L | 0.31µmol/L | 0.62µmol/L | 0.93µmol/L | 1.24µmol/L | 1.85µmol/L |

b Y=10.53X+141.97
R^2=0.98178
LOD=0.036µmol/L

c Y=10.22X+141.67
R^2=0.98166
LOD=0.034µmol/L

Fig. 9 Pesticide residue (methomyl) detection on the paper chip. **a** Optical images of the displayed color after the pesticide residue triggers the color reaction on the paper chip. **b** The linear relationship between the average RGB value and methomyl concentration. **c** The linear relationship between the average gray value and methomyl concentration

methodology based on the three-layered paper-based microfluidic chip is applied to analyze the real samples. The samples (upper brassica pekinensis, lower brassica chinensis) sprayed by methomyl to kill the insect pests and promote vegetable growth are pre-treated according to a certified standard (GB/T 5009.199–2003) for the detection as shown

in Fig. 10a. The testing samples are cut into small pieces to increase the contact area in the buffer solution. The multiple shaking can efficiently dissolve the pesticide residue into the buffer solution. A small volume of sample (12 µL) is added to the paper chip and triggers the detection reaction. The color reaction is also designed to be 15 min so as to complete

Table 1 LOD of profenofos and methomyl detected by previous methods

Detection substance	Detection method	LOD	Ref
Profenofos	Fluorescence polarization aptamer array	13.4 nM	[44]
	Fluorescence array	14 µM	[45]
	Surface-enhanced Raman scattering method	14 µM	[46]
	Gold-based nanobeacon probe for fluorescence	0.134 µM	[47]
	Paper-based microfluidic chips	55 nM	This work
Methomyl	Gas chromatography	0.02 ng mL^{-1}	[48]
	HPLC–DAD	0.005 ng mL^{-1}	[49]
	HPLC	1 ng mL^{-1}	[50]
	LC–MS/MS	0.0013 ng mL^{-1}	[51]
	Enzyme inhibition	0.235 µM	[52]
	Electrochemistry	0.02 µM	[53]
	Electrochemical detection	0.95 µM	[54]
	Fluorescence and Electrochemistry	2.23 µM	[55]
	Paper-based microfluidic chips	34 nM	This work

a

Cutting into 1cm square pieces and immensing them into 10 mL of buffer solution → Shaking 50 times, and after standing for 2 minutes, then dropping 12 μL of the solution into the detection chip →

Cutting into 1cm square pieces and immensing them into 10 mL of buffer solution → Shaking 50 times, and after standing for 2 minutes, then dropping 12 μL of the solution into the detection chip →

Detection reaction → Visual qualitation → Average Gray Value / Average RGB Value / Data quantification

b

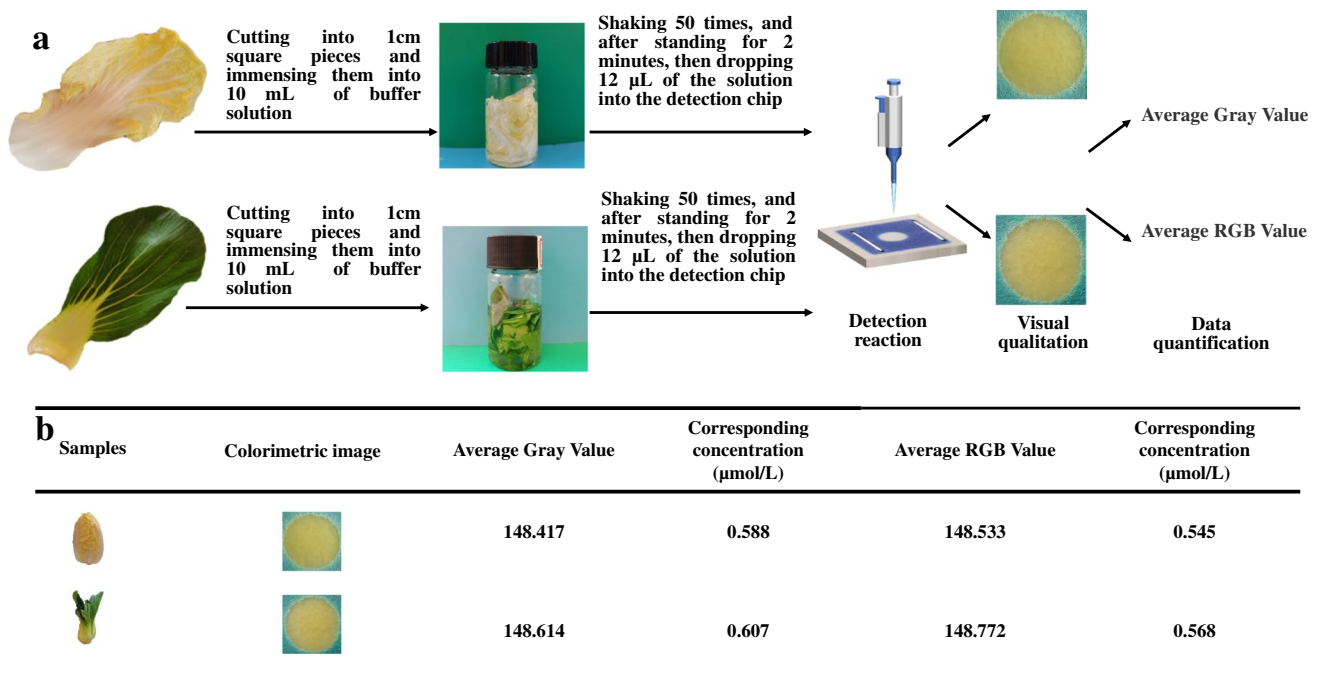| Samples	Colorimetric image	Average Gray Value	Corresponding concentration (μmol/L)	Average RGB Value	Corresponding concentration (μmol/L)
		148.417	0.588	148.533	0.545
		148.614	0.607	148.772	0.568

Fig. 10 Pesticide residue detection of real vegetable samples on the three-layered paper-based microfluidic chip. **a** The complete procedure of real vegetable sample detection, including sample pretreatment, analyte extraction, detection reaction and result analysis, upper brassica pekinensis, and lower brassica chinensis. **b** The detection results figured out according to the linear relationship between the average RGB value and methomyl concentration and the linear relationship between the average gray value and methomyl concentration

the detection reaction. The three-layered paper chip presents a brilliant yellow after completing the color reaction. By comparing the visual results with the colors in the standard pesticide residue detection, we can preliminarily judge the.

trace existence of the methomyl. Furthermore, we use the data process software to obtain the average gray value and average RGB value. Firstly, the buffer solution after immersing brassica pekinensis and brassica chinensis is used as the negative control sample in the detection process. The average gray value and average RGB value are 142.409 and 142.790, respectively. Therefore, 142.409 and 142.790 can be regarded as the background signals in the detection. For brassica pekinensis, the average gray value and average RGB value in the methomyl detection are 148.417 and 148.533, respectively. For brassica chinensis, the average gray value and average RGB value in the methomyl detection are 148.614 and 148.772, respectively. By comparing the above optical data (after deducting the background signals) with those in the calibration curves, the concentrations of methomyl originated from brassica pekinensis can be precisely calculated to be 0.588 μmol L^{-1} and 0.545 μmol L^{-1} (Fig. 10b). The concentrations of methomyl originated from brassica chinensis can be precisely calculated to be 0.607 μmol L^{-1} and 0.568 μmol L^{-1}. It should be pointed out that the methomyl concentrations calculated by the average gray value and average RGB value only generate small differences of -7.31% (for brassica pekinensis) and 6.43% (for brassica chinensis), demonstrating the excellent detection reliability by using the three-layered paper-based microfluidic chip. In the whole detection process, the trace reagents, the miniaturized paper chip, and mobile phone enable the portable detection of pesticide residue in restaurants, markets, homes, outdoor sites, or other health departments. What is more, the stability and corresponding storage condition of the paper-based chips are also important since it is designed to be an on-site use method. Therefore, we are now conducting experiments on this aspect, which will be presented in our future work.

Conclusion

In summary, we construct a novel smartphone-coupled three-layered paper-based microfluidic chip as a facile platform to detect the pesticides. The transport of the reaction flow is driven by the stereoscopic capillary force of the hydrophilic paper in the microfluidic chips without extra driving equipment. The detection mechanism is based on the enzyme inhibition reaction and the chromatic reaction. Owing to molecular-level interactions between the pesticides and the acetylcholine esterase and

the superior affinity between the detection reagents and hydrophilic paper substrate, the detection process can be completed within 10–15 min. The three-layered paper-based microfluidic chip presents colorimetric qualitative analysis by naked eyes. Furthermore, the colorimetric images can be easily captured by a smartphone. Two types of image processing results (average gray value and average RGB value) are figured out for the data quantitative analysis. The proposed detection method is also highly cost-effective owing to the cheap chip materials and economical reagent dosage. Based on the above merits, this work not only provides a simple and economic method for the detection of pesticides, but also makes a positive contribution to food safety and environmental protection.

Declarations

Competing interests The authors declare no competing interests.

References

1. Zhang M, Zeiss MR, Geng S. Agricultural pesticide use and food safety: California's model. J Integr Agric. 2015;14(11):2340–57. https://doi.org/10.1016/S2095-3119(15)61126-1.
2. Tournebize J, Chaumont C, Mander Ü. Implications for constructed wetlands to mitigate nitrate and pesticide pollution in agricultural drained watersheds. Ecol Eng. 2017;103:415–25. https://doi.org/10.1016/j.ecoleng.2016.02.014.
3. Lebov JF, Engel LS, Richardson D, Hogan SL, Sandler DP, Hoppin JA. Pesticide exposure and end-stage renal disease risk among wives of pesticide applicators in the Agricultural Health Study. Environ Res. 2015;143:198–210. https://doi.org/10.1016/j.envres.2015.10.002.
4. Bucur B, Munteanu F-D, Marty J-L, Vasilescu A. Advances in enzyme-based biosensors for pesticide detection. Biosensors. 2018;8(2):27. https://doi.org/10.3390/bios8020027.
5. Meyer A, Sandler DP, Beane Freeman LE, Hofmann JN, Parks CG. Pesticide exposure and risk of rheumatoid arthritis among licensed male pesticide applicators in the agricultural health study. Environ Health Perspect. 2017;125(7): 077010. https://doi.org/10.1289/EHP1013.
6. Stachniuk A, Fornal E. Liquid chromatography-mass spectrometry in the analysis of pesticide residues in food. Food Anal Methods. 2016;9(6):1654–65. https://doi.org/10.1007/s12161-015-0342-0.
7. Johnsen LG, Skou PB, Khakimov B, Bro R. Gas chromatography–mass spectrometry data processing made easy. J Chromatogr A. 2017;1503:57–64. https://doi.org/10.1016/j.chroma.2017.04.052.
8. Pico Y, Alfarhan AH, Barcelo D. How recent innovations in gas chromatography-mass spectrometry have improved pesticide residue determination: an alternative technique to be in your radar. TrAC, Trends Anal Chem. 2020;122: 115720. https://doi.org/10.1016/j.trac.2019.115720.
9. Chen J, Huang Y, Kannan P, Zhang L, Lin Z, Zhang J, et al. Flexible and adhesive surface enhance Raman scattering active tape for rapid detection of pesticide residues in fruits and vegetables. Anal Chem. 2016;88(4):2149–55. https://doi.org/10.1021/acs.analchem.5b03735.
10. Yang T, Doherty J, Guo H, Zhao B, Clark JM, Xing B, et al. Real-time monitoring of pesticide translocation in tomato plants by surface-enhanced Raman spectroscopy. Analytical chemistry. 2019;91(3):2093–9. http://orcid.org/0000-0003-4197-9262
11. Wang J, Zhang J, Wang J, Fang G, Liu J, Wang S. Fluorescent peptide probes for organophosphorus pesticides detection. J Hazard Mater. 2020;389: 122074. https://doi.org/10.1016/j.jhazmat.2020.122074.
12. Wang S, Wang J, Shang F, Wang Y, Cheng Q, Liu N. A GA-BP method of detecting carbamate pesticide mixture based on three-dimensional fluorescence spectroscopy. Spectrochim Acta Part A Mol Biomol Spectrosc. 2020;224: 117396. https://doi.org/10.1016/j.saa.2019.117396.
13. Peng J, Zhao N, Lin S, Wang W, Zhang M-J, Su Y-Y, et al. Smart microfluidic analogue of Wheatstone-bridge for real-time continuous detection with ultrasensitivity and wide dynamic range. Chem Eng J. 2021;407: 127138. https://doi.org/10.1016/j.cej.2020.127138.
14. Mu X-T, Li Y, Ju X-J, Yang X-L, Xie R, Wang W, et al. Microfluidic fabrication of structure-controlled chitosan microcapsules via interfacial cross-linking of droplet templates. ACS Appl Mater Interfaces. 2020;12(51):57514–25. https://doi.org/10.1021/acsami.0c14656.
15. Zhou L, Alcalde RE, Deng J, Zuniga B, Sanford RA, Fouke BW, et al. Impact of antibiotic concentration gradients on nitrate reduction and antibiotic resistance in a microfluidic gradient chamber. Sci Total Environ. 2021;779: 146503. https://doi.org/10.1016/j.scitotenv.2021.146503.
16. Youssef K, Archonta D, Kubiseski TJ, Tandon A, Rezai P. Microfluidic electric parallel egg-laying assay and application to in-vivo toxicity screening of microplastics using C. elegans. Science of The Total Environment. 2021;783:147055.https://doi.org/10.1016/j.scitotenv.2021.147055
17. Zheng L, Wang Y, Zhang Y, Fu Y, Yang Z, Fan Y, et al. EGFR inhibitors regulate Ca2+ concentration and apoptosis after PM2. 5 exposure based on a lung-mimic microfluidic system. Science of The Total Environment. 2021;761:143200.https://doi.org/10.1016/j.scitotenv.2020.143200
18. Baranger C, Pezron I, Lins L, Deleu M, Le Goff A, Fayeulle A. A compartmentalized microsystem helps understanding the uptake of benzo [a] pyrene by fungi during soil bioremediation processes. Sci Total Environ. 2021;784: 147151. https://doi.org/10.1016/j.scitotenv.2021.147151.
19. Bai Y, Henry J, Campana O, Wlodkowic D. Emerging prospects of integrated bioanalytical systems in neuro-behavioral toxicology. Science of The Total Environment. 2020:143922.
20. Wang X, Yu Y, Yang C, Shao C, Shi K, Shang L, et al. Microfluidic 3D printing responsive scaffolds with biomimetic enrichment channels for bone regeneration. Advanced Functional Materials. 2021:2105190.https://doi.org/10.1016/j.scitotenv.2020.143922
21. Huang D, Zhang X, Zhao C, Fu X, Zhang W, Kong W, et al. Ultrasound-responsive microfluidic microbubbles for combination tumor treatment. Advanced Therapeutics. 2021;4(7):2100050. https://doi.org/10.1002/adtp.202100050.
22. Zhao Y, Hu X-g, Hu S, Peng Y. Applications of fiber-optic biochemical sensor in microfluidic chips: a review. Biosensors and Bioelectronics. 2020:112447.https://doi.org/10.1016/j.bios.2020.112447

23. Lin H, Tan J, Zhu J, Lin S, Zhao Y, Yu W, et al. A programmable epidermal microfluidic valving system for wearable biofluid management and contextual biomarker analysis. Nat Commun. 2020;11(1):1–12. https://doi.org/10.1038/s41467-020-18238-6.

24. Rodrigues RO, Sousa PC, Gaspar J, Bañobre-López M, Lima R, Minas G. Organ-on-a-chip: a preclinical microfluidic platform for the progress of nanomedicine. Small. 2020;16(51):2003517. https://doi.org/10.1002/smll.202003517.

25. Urbanska M, Muñoz HE, Bagnall JS, Otto O, Manalis SR, Di Carlo D, et al. A comparison of microfluidic methods for high-throughput cell deformability measurements. Nat Methods. 2020;17(6):587–93. https://doi.org/10.1038/s41592-020-0818-8.

26. Mo Y, Lu Z, Rughoobur G, Patil P, Gershenfeld N, Akinwande AI, et al. Microfluidic electrochemistry for single-electron transfer redox-neutral reactions. Science. 2020;368(6497):1352–7. https://doi.org/10.1126/science.aba3823.

27. Berlanda SF, Breitfeld M, Dietsche CL, Dittrich PS. Recent advances in microfluidic technology for bioanalysis and diagnostics. Anal Chem. 2020;93(1):311–31. https://doi.org/10.1021/acs.analchem.0c04366.

28. Moreddu R, Elsherif M, Adams H, Moschou D, Cordeiro MF, Wolffsohn JS, et al. Integration of paper microfluidic sensors into contact lenses for tear fluid analysis. Lab Chip. 2020;20(21):3970–9. https://doi.org/10.1039/d0lc00438c.

29. Sachdev A, Samanta P, Kumar V, Kandhal K, Matai I. PMAA-CeO 2 nanoparticle-based paper microfluidic device with customized image processing software for antioxidant assay. Anal Bioanal Chem. 2020;412(29):8197–209. https://doi.org/10.1007/s00216-020-02960-7.

30. Fukuyama M, Mott DM, Koseki Y, Kasai H, Hibara A. Organic nanocrystal enrichment in paper microfluidic analysis. Sens Actuators, B Chem. 2021;333: 129548. https://doi.org/10.1016/j.snb.2021.129548.

31. Trofimchuk E, Hu Y, Nilghaz A, Hua MZ, Sun S, Lu X. Development of paper-based microfluidic device for the determination of nitrite in meat. Food Chem. 2020;316: 126396. https://doi.org/10.1016/j.foodchem.2020.126396.

32. Snyder SA, Boban M, Li C, VanEpps JS, Mehta G, Tuteja A. Lysis and direct detection of coliforms on printed paper-based microfluidic devices. Lab Chip. 2020;20(23):4413–9. https://doi.org/10.1039/d0lc00665c.

33. Lee M, Oh K, Choi H-K, Lee SG, Youn HJ, Lee HL, et al. Subnanomolar sensitivity of filter paper-based SERS sensor for pesticide detection by hydrophobicity change of paper surface. ACS sensors. 2018;3(1):151–9. https://doi.org/10.1021/acssensors.7b00782.

34. Kwon G, Kim J, Kim D, Ko Y, Yamauchi Y, You J. Nanoporous cellulose paper-based SERS platform for multiplex detection of hazardous pesticides. Cellulose. 2019;26(8):4935–44. https://doi.org/10.1007/s10570-019-02427-8.

35. Nouanthavong S, Nacapricha D, Henry CS, Sameenoi Y. Pesticide analysis using nanoceria-coated paper-based devices as a detection platform. Analyst. 2016;141(5):1837–46. https://doi.org/10.1039/c5an02403j.

36. Wang T, Reid RC, Minteer SD. A Paper-based mitochondrial electrochemical biosensor for pesticide detection. Electroanalysis. 2016;28(4):854–9. https://doi.org/10.1002/elan.201500487.

37. Tang X, Zhang Q, Zhang Z, Ding X, Jiang J, Zhang W, et al. Rapid, on-site and quantitative paper-based immunoassay platform for concurrent determination of pesticide residues and mycotoxins. Anal Chim Acta. 2019;1078:142–50. https://doi.org/10.1016/j.aca.2019.06.015.

38. Shrivas K, Patel S, Thakur SS, Shankar R. Food safety monitoring of the pesticide phenthoate using a smartphone-assisted paper-based sensor with bimetallic Cu@ Ag core–shell nanoparticles.

39. Kim JY. Carbon nanotube-reinforced thermotropic liquid crystal polymer nanocomposites. Materials. 2009;2(4):1955–74. https://doi.org/10.3390/ma2041955.

40. Kushwaha M, Verma S, Chatterjee S. Profenofos, an acetylcholinesterase-inhibiting organophosphorus pesticide: a short review of its usage, toxicity, and biodegradation. J Environ Qual. 2016;45(5):1478–89. https://doi.org/10.2134/jeq2016.03.0100.

41. Shalaby M, El Zorba H, Ziada RM. Reproductive toxicity of methomyl insecticide in male rats and protective effect of folic acid. Food Chem Toxicol. 2010;48(11):3221–6. https://doi.org/10.1016/j.fct.2010.08.027.

42. Yang G-P, Zhao Y-H, Lu X-L, Gao X-C. Adsorption of methomyl on marine sediments. Colloids Surf, A. 2005;264(1–3):179–86. https://doi.org/10.1016/j.colsurfa.2005.05.018.

43. Rodrigues FT, Marchioni E, Lordel-Madeleine S, Kuntz F, Villavicencio ALCH, Julien-David D. Degradation of profenofos in aqueous solution and in vegetable sample by electron beam radiation. Radiat Phys Chem. 2020;166: 108441. https://doi.org/10.1016/j.radphyschem.2019.108441.

44. Zhang C, Wang L, Tu Z, Sun X, He Q, Lei Z, Xu C, Liu Y, Zhang X, Yang J. Organophosphorus pesticides detection using broad-specific single-stranded DNA based fluorescence polarization aptamer assay. Biosens Bioelectron. 2014;55:216–9. https://doi.org/10.1016/j.bios.2013.12.020.

45. Li W, Hua Y, Hong-Qing S, Dan-Dan W. Aptamer-based fluorescence assay for detection of Isocarbophos and Profenofos. Chin J Anal Chem. 2016;44(5):799–803. https://doi.org/10.1016/j.bios.2013.12.020.

46. Pang S, Labuza TP, He L (2014) Development of a single aptamer-based surface enhanced Raman scattering method for rapid detection of multiple pesticides. Analyst 139 (8):1895–1901. https://pubs.rsc.org/en/content/articlehtml/2014/an/c3an02263c

47. Dou X, Chu X, Kong W, Luo J, Yang M. A gold-based nanobeacon probe for fluorescence sensing of organophosphorus pesticides. Anal Chim Acta. 2015;891:291–7. https://doi.org/10.1016/j.aca.2015.08.012.

48. Pease H, Kirkland J (1968) Determination of methomyl residues using microcoulometric gas chromatography. Journal of Agricultural and Food Chemistry 16 (4):554–557. https://doi.org/10.1021/jf60158a004

49. Malhat F, Watanabe H, Youssef A. Degradation profile and safety evaluation of methomyl residues in tomato and soil. Hellenic Plant Protection Journal. 2015;8(2):55–62. https://doi.org/10.1515/hppj-2015-0008.

50. Alawi M, Rüssel H. Determination of methomyl and methomyl-oxime in fruit crops and water by HPLC. Fresenius' Zeitschrift für analytische Chemie. 1981;309(1):8–12. https://doi.org/10.1007/BF00493444.

51. Rasolonjatovo MA, Cemek M, Cengiz MF, Ortaç D, Konuk HB, Karaman E, Kocaman AT, Göneş S. Reduction of methomyl and acetamiprid residues from tomatoes after various household washing solutions. Int J Food Prop. 2017;20(11):2748–59. https://doi.org/10.1080/10942912.2016.1250099.

52. Zapp E, Brondani D, Vieira IC, Scheeren CW, Dupont J, Barbosa AM, Ferreira VS. Biomonitoring of methomyl pesticide by laccase inhibition on sensor containing platinum nanoparticles in ionic liquid phase supported in montmorillonite. Sens Actuators, B Chem. 2011;155(1):331–9. https://doi.org/10.1016/j.snb.2011.04.015.

53. Abbaci A, Azzouz N, Bouznit Y. Development and validation of a new sensor for methomyl detection. Anal Methods. 2013;5(15):3663–8. https://doi.org/10.1039/C3AY40332G.

54. Cesarino I, Moraes FC, Lanza MR, Machado SA. Electrochemical detection of carbamate pesticides in fruit and vegetables

with a biosensor based on acetylcholinesterase immobilised on a composite of polyaniline–carbon nanotubes. Food Chem. 2012;135(3):873–9. https://doi.org/10.1016/j.foodchem.2012.04.147.

55. Azab HA, Duerkop A, Mogahed E, Awad F, Abd El Aal R, Kamel RM. Fluorescence and electrochemical sensing of pesticides methomyl, aldicarb and prometryne by the luminescent europium-3-carboxycoumarin probe. J Fluoresc. 2012;22(2):659–76. https://doi.org/10.1007/s10895-011-1002-4.

Publisher's note Springer Nature remains neutral with regard to jurisdictional claims in published maps and institutional affiliations.

Hongjiao Wu is currently a postgraduate student of the School of Materials and Energy, Guangdong University of Technology. Her research mainly focuses on the design and manufacture of paper-based microfluidic chip and its application in point-of-care testing.

Jiaqi Chen is a postgraduate student of the School of Materials and Energy, Guangdong University of Technology. She obtained a bachelor's degree in polymer materials and engineering from Guangdong University of Technology in 2021. Her main research topic is the design of biomedical materials and their application in point-of-care testing.

Yi Yang is an undergraduate student of the School of Materials and Energy, Guangdong University of Technology. Her main research topic is the preparation of biomedical materials and their application in point-of-care testing.

Weitai Yu is a postgraduate student of the School of Materials and Energy, Guangdong University of Technology. He obtained a bachelor's degree in polymer materials and engineering from Guangdong University of Technology in 2015. He mainly focuses on the design, fabrication, and application of advanced functional materials.

Ying Chen is Professor at the Guangdong University of Technology, also Dean of the School of Materials and Energy and Executive Director of Guangdong Provincial Key Laboratory on Functional Soft Condensed Matter. She received her PhD degree in chemical engineering from South China University of Technology in 2003. She joined Guangdong University of Technology as a lecturer in 1994, and was promoted to Professor in 2008. Her research interests focus on the design, fabrication, and application of advanced functional materials.

Pengcheng Lin is Associate Professor of Guangdong Provincial Key Laboratory on Functional Soft Condensed Matter (Guangdong University of Technology). He received his PhD degree in polymer chemistry and physics from Northeastern University in 2016. He worked as a visiting scholar in City University of Hong Kong from 2018 to 2019. His research interests focus on microfluidic technology and point-of-care testing.
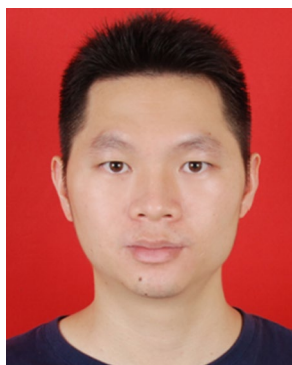
Ke Liang is Manager of the R&D Centre of Guangdong Dayuan Oasis Food Safety Technology Co., Ltd. He obtained a bachelor's degree in biotechnology from South China Agricultural University in 2012. His research interests focus on the development and application of food safety rapid detection technology.